PAN
ARCHIVES OF ACOUSTICS
Vol. **45**, No. 1, pp. 3–9 (2020)
DOI: 10.24425/aoa.2019.129736

CC BY SA

Research Paper

Effect of Emergence Angle on Acoustic Transmission in a Shallow Sea

Yanyang LU[(1),(2)], Kunde YANG[(1),(2)*], Hong LIU[(1),(2)], Chunlong HUANG[(1),(2)]

[(1)] *School of Marine Science and Technology*
Northwestern Polytechnical University
Xi'an, 710072, China; e-mail: cqjndys@sina.com; {liuhong_2017, hcl0207}@mail.nwpu.edu.cn
*Corresponding Author e-mail: ykdzym@nwpu.edu.cn

[(2)] *Key Laboratory of Ocean Acoustics and Sensing (Northwestern Polytechnical University)*
Ministry of Industry and Information Technology
Xi'an, 710072, China

(*received September 22, 2018; accepted October 30, 2019*)

In this study, the effect of the emergence angle of a source array on acoustic transmission in a typical shallow sea is simulated and analyzed. The formula we derived for the received signal based on the Normal Mode indicates that the signal is determined by the beamform on the modes of all sources and the samplings of all modes at the receiving depth. Two characteristics of the optimal emergence angle (OEA) are obtained and explained utilizing the aforementioned derived formula. The observed distributions of transmission loss (TL) for different sources and receivers are consistent with the obtained characteristics. The results of this study are valuable for the development and design of active sonar detection.

Keywords: underwater acoustic; emergence angle; transmission loss; active sonar detection.

1. Introduction

The majority of studies on array beamforming have focused on the beamforming application of a receiver array. In recent years, the advancement of multistatic sonar (Sheng *et al.*, 2014) and the continuous development of active sonar (Zhao, 2013) technologies have motivated considerable research on the signal transmission of the active sonar array. This has highlighted the need for more thorough investigations on the acoustic beam output.

The detection range of the active sonar serves as the most important reference factor in studying the active sonar (Cable, 2006). In order to improve the detection range of active sonar, commonly used methods have been adopted in an effort to increase the sound source level of the active sonar and improve the signal-processing capability of the receiver. Methods to improve the sound source level are primarily aimed at enhancing the sound source power and developing the directivity factor of a sound source.

The development of acoustic engineering in recent years has broadened the investigation of the acoustic physical field. Acoustic transmission is affected by factors underlying reflections of the sea bottom and surface (Yang *et al.*, 2017), the same as the presence of a reliable acoustic path (Duan *et al.*, 2012), the convergence zone (Urick, 1965), and the deep ocean acoustic channel (Hale, 1961). The effects are primarily reflected in the arrival time, arrival angle, acoustic energy, and forward scattering. Many scholars have exploited these effects to investigate localization (Yang, 2017; Lei, 2016; Duan, 2014), acoustic inversion (Yang *et al.*, 2004; 2007), error analysis (Yang, 2016), depth estimation (Yang *et al.*, 2016), forward scattering (He *et al.*, 2015; 2016; Lei *et al.*, 2012; 2014), and noise reduction (Xia *et al.*, 2016; Xiao, Yang, 2016). Additionally, sound speed profiles (SSP) and submarine topography also significantly affect acoustic transmission (Katsnelson *et al.*, 2011). Different source and receiver positions can result in various acoustic transmission effects. The sensibility of transmission loss (TL) with varying source and receiver depths in a shallow sea during the summer was investigated by Herstein, the results of which were compared with the results of an investigation by Cole (Herstein *et al.*, 2006; Cole, Podeszwa, 1967). The latter utilized a ray model and the experimental data

of a shallow water to study the TL of downward refraction. The results indicated that both SSP and the bottom loss coefficient play primary roles in downward refraction conditions (Cole, Podeszwa, 1967). Colen (1977) conducted a series of experiments investigating shallow-water propagations under downward refraction conditions. Hall (1975) developed the transmission characteristics of a typical mixed layer and determined that the acoustic energy is larger in the mixed layer as compared to under a thick mixed layer. Zhang (2016) derived an averaged shallow-water TL formula that considers spreading loss, water absorption, surface scattering, and sea bottom absorption. The aforementioned studies have all indicated that the effects of signal form and physical field play important roles in TL. Therefore, adjusting the emergence angle can enhance the detection range under certain conditions. Thus, here we conduct a relevant study on the basis of the aforementioned considerations.

The structure of this paper is as follows. The algorithm for the acoustic beam output is introduced in Sec. 2, which also contains a discussion on the derivation of the formula for the acoustic signal with Normal Mode. Two characteristics of OEA from the simulation of TL with different source and receiver positions are described in Sec. 3; the formula derived in Sec. 2 is utilized in order to explain the characteristics. A simulation in Sec. 4 verifies the characteristics and provides some conclusions and advice. The conclusions drawn from this study are then discussed in Sec. 5.

2. Algorithm

A vertical linear array of sound sources is illustrated in Fig. 1. The reference source is set as the lowest source and is denoted by 0. The sources are numbered from 0 to M incrementally from the lowest to the highest source (the number of source array elements is $M+1$). The directivity in a certain orientation means that signals from a source array have equiphase surfaces in a specific orientation. The red line in Fig. 1 represents an equiphase surface with a directional angle θ. The signals for all of the sound sources arrive on the equiphase surface at time t_m, $m = 0, 1, 2, \ldots, M$, where t_0 is the arrival time of the signal from the reference source (number-0 source).

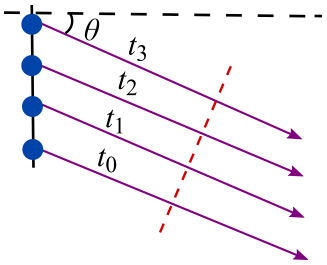

Fig. 1. Schematic of transmitting signals.

The signal for the reference source is assumed to be $s_0(t) = s(t)$, and it is $s(t - t_0)$ when it arrives at the equiphase surface. To enable all of the signals to be $s(t - t_0)$ upon their arrival at the equiphase surface, the signals for the other sources are derived as $s_m(t) = s(t + \tau_m)$, $m = 1, 2, ..., M$, where $\tau_m = t_m - t_0 = \frac{d_m \sin\theta}{c}$, $m = 0, 1, 2, ..., M$, and d_m is the distance between the number-m and number-0 sources. All of the source signals are represented as follows:

$$s_m(t) = s(t + \tau_m), \qquad m = 0, 1, 2, ..., M. \tag{1}$$

If the Fourier transformation of the original signal $s(t)$ is $S(\omega) = \int_{-\infty}^{+\infty} s(t) e^{-jwt}\,\mathrm{d}t$ (Fast Fourier transforms (FFT) are often used in practical calculations), then the Fourier transformation of all of the sources are:

$$X(\omega, \theta) = S(\omega) \cdot w(\theta), \tag{2}$$

and

$$w(\theta) = \left[1, e^{j2\pi f \tau_1}, e^{j2\pi f \tau_1} \ldots e^{j2\pi f \tau_M}\right]$$
$$= \left[1, e^{j2\pi f d_0 \sin\theta/c}, e^{j2\pi f d_1 \sin\theta/c} \ldots e^{j2\pi f d_M \sin\theta/c}\right], \tag{3}$$

$X(w, \theta)$ is a $1 \times (M + 1)$ vector composed of each element signal.

The signal in the acoustic field $p(t)$ can be represented by the source signal $x(t)$ and the channel function $h(t)$ as:

$$p(t) = x(t) \otimes h(t), \tag{4}$$

with $\otimes$ meaning convolution. This can be transformed into the Fourier transformation (Zhang *et al.*, 2015)

$$P(\omega) = X(\omega) \cdot H(\omega), \tag{5}$$

where

$$X(\omega) = \int_{-\infty}^{+\infty} x(t) e^{-jwt}\,\mathrm{d}t,$$

$$H(\omega) = \int_{-\infty}^{+\infty} h(t) e^{-jwt}\,\mathrm{d}t$$

are the Fourier transformation of $x(t)$, $h(t)$, respectively. Equation (5) can be derived in the following vector form:

$$P(\omega) = X(\omega) \odot H(\omega), \tag{6}$$

where $H(\omega)$ is a $1 \times (M + 1)$ vector and $\odot$ is the Hadamard product. Utilizing Eq. (2), signals from all of the sources can be written as:

$$P(\omega, \theta) = S(\omega) \cdot w(\theta) \odot H(\omega), \tag{7}$$

where $P(\omega, \theta)$ is a $1 \times (M + 1)$ vector and the final received signal is the accumulation of all of the signals, represented as:

$$Y(\omega, \theta) = \sum P(\omega, \theta). \tag{8}$$

Formula (8) can also be written as:

$$Y(\omega,\theta) = S(\omega)\cdot w(\theta)\cdot H^{\mathrm{T}}(\omega). \tag{9}$$

The Normal-Mode has been widely used in recent years in computational mode. In this study, the Normal-Mode solution is used in order to analyze the received signals. The Normal-Mode solution of sound pressure in $r = (r,z)$ from the Helmholtz equation is (source $r_s = (0,z_s)$)

$$p(r,z) = \frac{i}{\rho(z_s)\sqrt{8\pi r}} e^{\frac{-i\pi}{4}} \sum_{n=1}^{N} \psi_n(z_s)\psi_n(z)\frac{e^{ik_{r,n}r}}{\sqrt{k_{r,n}}}, \tag{10}$$

where $\rho(z_s)$ is the density at the source position, and $k_{r,n}$ and $\psi_n(z)$ are the eigenvalue and eigenfunction of the n-th mode, respectively (Jensen *et al.*, 1994, pp. 338–340), N is the number of effective modes. In Eq. (5), making $X(\omega) = 1$, meaning only one source with unit signal,

$$p(r,z,\omega) = 1\cdot H(r,z,\omega) = \frac{i}{\rho(z_s)\sqrt{8\pi r}} e^{\frac{-i\pi}{4}} \cdot \sum_{n=1}^{N} \psi_n(z_s)\psi_n(z)\frac{e^{ik_{r,n}r}}{\sqrt{k_{r,n}}}. \tag{11}$$

Accordingly, the channel function is:

$$H(r,z,\omega) = \frac{i}{\rho(z_s)\sqrt{8\pi r}} e^{\frac{-i\pi}{4}} \cdot \sum_{n=1}^{N} \psi_n(z_s)\psi_n(z)\frac{e^{ik_{r,n}r}}{\sqrt{k_{r,n}}}. \tag{12}$$

Formula (9) can then be expressed as:

$$Y(\omega,\theta) = S(\omega)\cdot w(\theta) \cdot \begin{bmatrix} \sum_{n=1}^{N} \frac{ie^{-i\pi/4}}{\rho(z_{s0})\sqrt{8\pi(r-r_{s0})}}\psi_n(z_{s0})\frac{e^{ik_{r,n}(r-r_{s0})}}{\sqrt{k_{r,n}}}\cdot\psi_n(z) \\ \sum_{n=1}^{N} \frac{ie^{-i\pi/4}}{\rho(z_{s1})\sqrt{8\pi(r-r_{s1})}}\psi_n(z_{s1})\frac{e^{ik_{r,n}(r-r_{s1})}}{\sqrt{k_{r,n}}}\cdot\psi_n(z) \\ \vdots \\ \sum_{n=1}^{N} \frac{ie^{-i\pi/4}}{\rho(z_{sM})\sqrt{8\pi(r-r_{sM})}}\psi_n(z_{sM})\frac{e^{ik_{r,n}(r-r_{sM})}}{\sqrt{k_{r,n}}}\cdot\psi_n(z) \end{bmatrix}. \tag{13}$$

Introducing the following:

$$A_n = \frac{ie^{\frac{-i\pi}{4}}}{\rho(z_{sm})\sqrt{8\pi(r-r_{sm})}}\psi_n(z_{sm})\frac{e^{ik_{r,n}(r-r_{sm})}}{\sqrt{k_{r,n}}}, \tag{14}$$

indicates the n-th mode amplitude of source sm (Bogart, Yang, 1994), while $(r - r_{sm})$ means distance from receiver to source sm. Normally, if the array is vertical linear array, the sound source distance r_{sm} is always set to 0. The vector symbol is introduced as

$$A_n = [A_n(s_0), A_n(s_1), ..., A_n(s_M)]^{\mathrm{T}}, \tag{15}$$

denoting the n-th mode amplitude vector of all source elements, T means transpose. Therefore, formula (13) can be written as:

$$Y(\omega,\theta) = S(\omega)\cdot\sum_{n=1}^{N}(w(\theta)A_n\cdot\psi_n(z)), \tag{16}$$

where $\psi_n(z)$ is the sampling of the n-th mode at the receiving depth.

Introducing

$$B_n = w(\theta)A_n, \tag{17}$$

which means the beamform on the n-th mode of all of the source elements. Formula (16) can also be defined as:

$$Y(\theta) = S(\omega)\cdot\sum_{n=1}^{N}(B_n\cdot\psi_n(z)). \tag{18}$$

The received signal is, therefore, determined by the beamform on the modes of all of the sources and the samples of all modes at the receiving depth. The two factors are relative to the depth.

3. Analysis of the signals' characteristics

An SSP obtained from historical data of the East China Sea is shown in Fig. 2. A negative gradient layer (NGL) in an SSP is a typical characteristic of a shallow sea. The sea depth is 130 m. The density of the bottom sediment is 1.39 g/cm^3, and the speed is 1570 m/s.

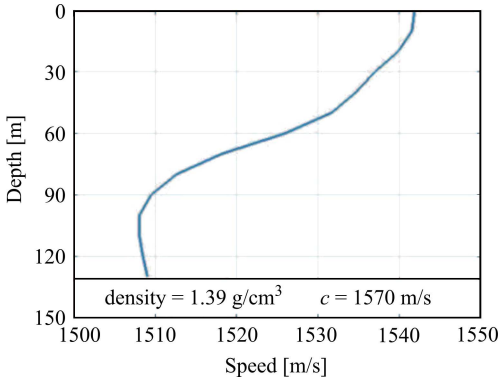

Fig. 2. SSP of the historical data.

The source array is a 17-element vertical linear array (17 sources) spaced at equal interval of 1.5 m. The frequency is 500 Hz.

A distance of 20 km is selected, and source depths are set at 15, 60, and 100 m (henceforth, the source depth means the depth of the center hydrophone of the vertical linear array). The Kraken model is used to simulate the acoustical field. We simulate the TL distribution in the depth-angle plane, as illustrated in Fig. 3, and verify transmission performances by TL. A large TL implies a poor transmission performance. The formula of the transmission loss is: $\mathrm{TL} = -10\log_{10}\left(\frac{I_r}{I_s}\right)$.

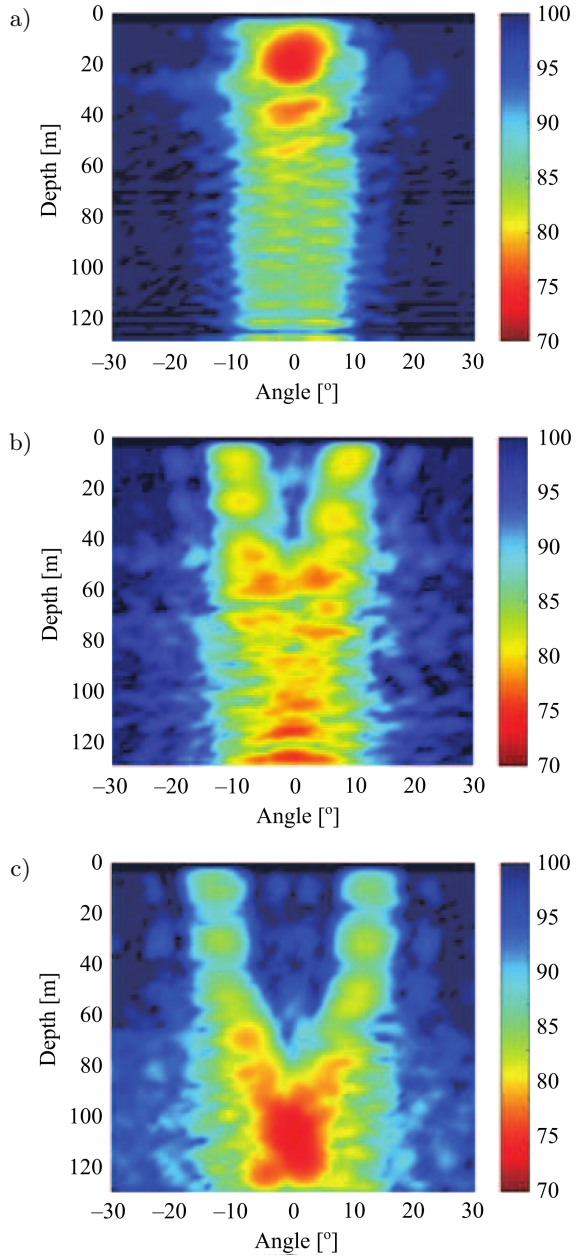

Fig. 3. TL distribution with a changing receiving depth: a) source depth of 15 m; b) source depth of 60 m; c) source depth of 100 m.

I_r is the acoustic intensity of the receiver and I_s is the acoustic intensity of source. The TL can be calculated directly using the sound field model in the simulation, so the specific calculations of TL are not included in this paper.

The result of this simulation shows that the TL distribution at receiving depths has several alternating dark and bright streaks, which means that the signal energy changes at a similar periodicity along depths.

The OEA deviates from 0° in some shallow depths when the source is deeper, and this phenomenon becomes more pronounced with an increase in the source depth. Owing to this phenomenon, we plot the TL distribution with various source depths in Fig. 4. The distance is selected to be 20 km, and the receiving depths are set to 15 and 60 m. The result confirms that the OEA deviates further from 0° as the source depth increases.

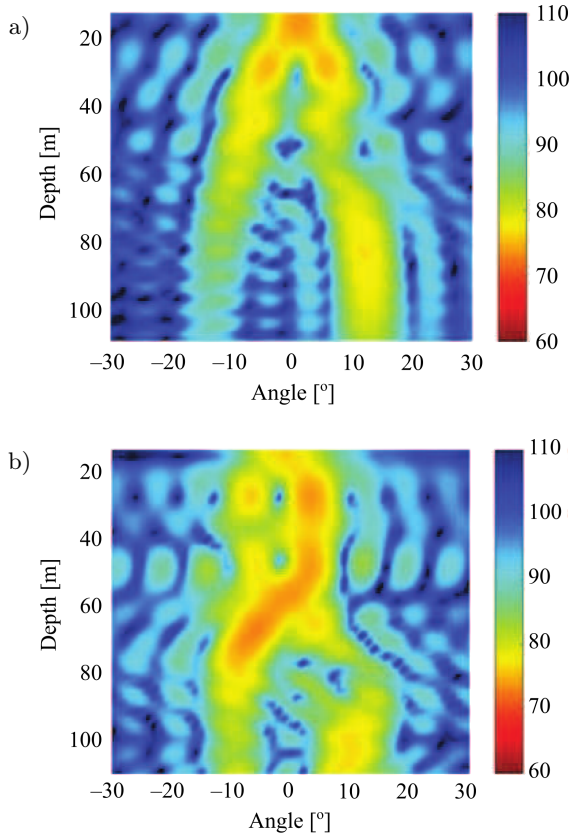

Fig. 4. TL distribution with a changing source depth: a) receiving depth of 15 m; b) receiving depth of 60 m.

The two main characteristics are summarized in Figs 3 and 4:

1) The TL distribution exhibits alternating dark and bright streaks with changes in the receiving depth.
2) In some shallow depths, the OEA is shown to deviate further from 0° with an increasing source depth.

The two characteristics are explained using the derived formula obtained in Sec. 2. Using Eq. (18) in order to explain characteristic 1: $\psi_n(z)$ is the n-th mode function. The number of effective modes reaches up to 20 under a given SSP at frequency of 500 Hz. Figure 5 depicts several modes. The mode function has analogous sinusoidal motion at all depths. The mode function may be large at certain depths and very small (even 0) at other depths. If a certain mode function is calculated, as presented in Eq. (19) (a special case of Eq. (18) when $N = 1$), the dark and bright streaks appear regularly. All of the mode functions affect one an-

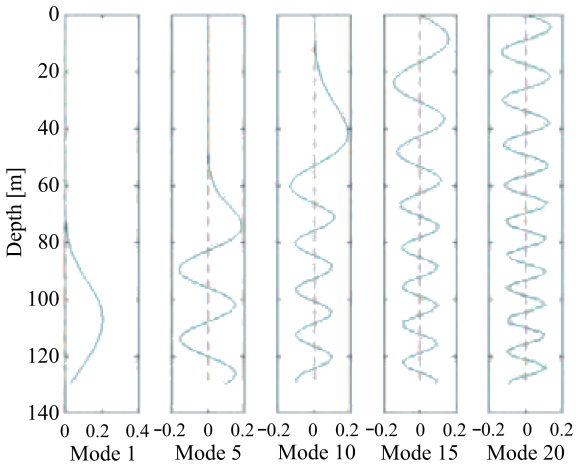

Fig. 5. Schematic of the mode functions.

other, hence weakening the streaks; this phenomenon is the underlying cause of the characteristic 1

$$y_n(\theta) = S(\omega) \cdot B_n \cdot \psi_n(z). \tag{19}$$

Characteristic 2 is related to the source depth. Therefore, we can deduce that characteristic 2 can be determined by B_n in Eq. (18). Using the Kraken model, we can obtain the mode amplitude (A_n shown in Eq. (14)) for all of the effective modes at all depths. B_n is the beamform output on the n-th mode of all sources, as shown in Eq. (17). We compute and plot all B_n, $n = 1, 2, ..., 20$ (uniformized) in Fig. 6 at a mode-angle plane. The source depths are set to 15, 60, and 100 m.

The OEA distributions of B_n are different in all modes, as shown in Fig. 6. Low modes are only motivated in a deep layer (Fig. 5); for example, the first five modes are not motivated at the depth of 60 m. Therefore, no obvious high-energy point is observed within the first five modes in Fig. 6b. The source at the 60 m depth cannot motivate the first five modes, and the high-energy points of the beamform appear in the high modes. Conversely, the source at the deepest layer motivates all of the modes, as shown in Fig. 6c, and the high-energy points of the beamform, which represent the appropriate emergence angles, are conspicuous in each mode. Consequently, characteristic 2 is a result of more modes taking effect in deeper layers.

4. Verification and application advice

Considering the influence of the emergence angle of the sound source array on sound propagation, we simulate some conditions using different sources and receivers. The SSP is shown in Fig. 2, and the simulation conditions are the same as above. Taking characteristic 2 into account, the two deeper depths of 60 m and 100 m were chosen for the sound source, and the

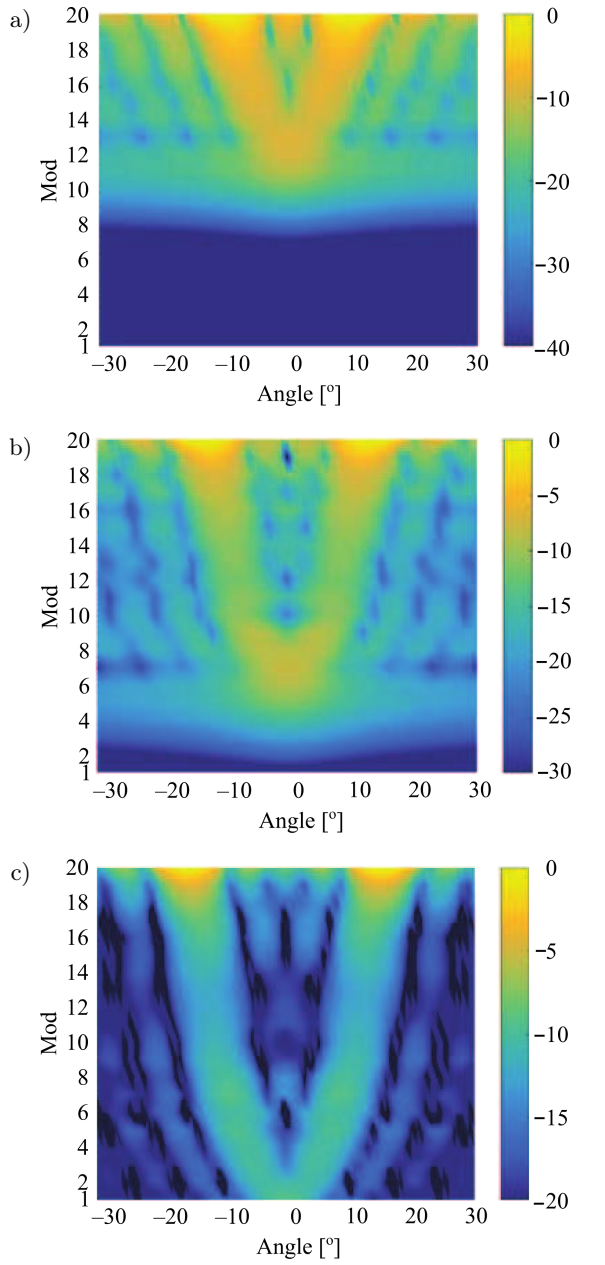

Fig. 6. Beamform output on all modes of the source array: a) source depth of 15 m; b) source depth of 60 m; c) source depth of 100 m.

two shallower depths of 15 m and 60 m were chosen for the receiver. The resulting TL distribution is shown in Fig. 7.

The simulation results are consistent with characteristic 2; the most prominent deviation from 0° was found in the conditions depicted in Fig. 7c, and there is no obvious deviation from 0° in the conditions depicted in Fig. 7b. Thus, it can be concluded that the deeper the sound source and the shallower the receiver, it is more likely that the OEA will deviate from 0°.

These results are very valuable for the development and design of underwater active detection technology. For example, in a typical shallow sea, when the active

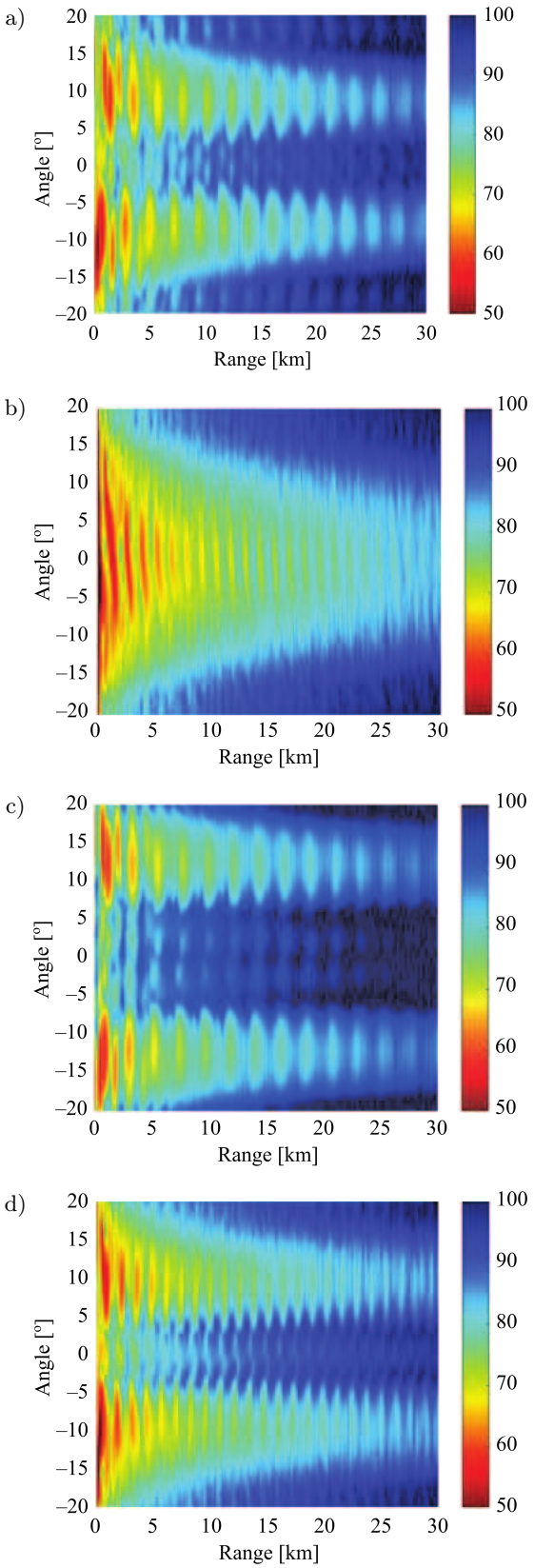

Fig. 7. Distribution of TL in different conditions (SD is the abbreviation of source-depth and RD is the abbreviation of receiver-depth): a) SD – 60 m and RD – 15 m; b) SD – 60 m and RD – 60 m; c) SD – 100 m and RD – 15 m; d) SD – 100 m and RD – 60 m.

sonar is placed in a shallow water layer, controlling its emergence angle at 0° it can achieve optimal output performance; when the active sonar is placed close to the sea floor, the emergence angle of the signal that has deviated from 0° can result in a larger detectable distance. In different marine environments, with detection targets at different depths, it is not a simple omnidirectional emission acoustic signal that makes use of the detection target. Instead, the optimal signal emergence angle according to the actual situation should be identified in order to achieve the maximum detection distance.

5. Conclusions

In this study, we simulated and analyzed the effect of the emergence angle of a source array on acoustic transmission in a typical shallow sea. The formula we derived for the received signal based on the Normal Mode indicates that the signal is determined by the beamform on the modes of all sources and the samples of all modes at the receiving depth. Then, simulations were carried out to determine the TL distributions for various receiving and source depths. Two characteristics of the OEA were obtained and subsequently explained using the aforementioned derived formula. It has been shown that the distributions of TL using different sources and receivers are consistent with the obtained characteristics. The results of this study regarding the effect of the emergence angle on TL under certain conditions are valuable for practical engineering, such as active sonar design.

References

1. Bogart C.W., Yang T.C. (1994), Source localization with horizontal arrays in shallow water: Spatial sampling and effective aperture, *Journal of the Acoustical Society of America*, **96**(3): 1677–1686, doi: 10.1121/1.410247.

2. Cable P.G. (2006), A method to predict active sonar detection range in uncertain shallow water environments, *Journal of the Acoustical Society of America*, **119**(5): 3426, doi: 10.1121/1.4786870.

3. Cohen J.S., Cole B.F. (1977), Shallow-water propagation under downward-refraction conditions. II, *Journal of the Acoustical Society of America*, **61**(1): 213–217, doi: 10.1121/1.381259.

4. Cole B.F., Podeszwa E.M. (1967), Shallow-water propagation under downward-refraction conditions, *Journal of the Acoustical Society of America*, **41**(6): 1479–1484, doi: 10.1121/1.1910510.

5. Duan R., Yang K., Ma Y. (2012), Research on reliable acoustic path: Physical properties and a source localization method, *Chinese Physics B*, **21**(12): 276–289, doi: 10.1088/1674-1056/21/12/124301.

6. Duan R., Yang K., Ma Y., Yang Q., Li H. (2014), Moving source localization with a single hydrophone using multipath time delays in the deep ocean, *Journal of the Acoustical Society of America*, **136**(2): 159–165, doi: 10.1121/1.4890664.
7. Hale F.E. (1961), Long-range sound propagation in the deep ocean,*Journal of the Acoustical Society of America*, **33**(4): 456–464, doi: 10.1121/1.1908691.
8. Hall M. (1975), Studies of sound transmission in the ocean mixed layers,*Journal of the Acoustical Society of America*, **57**(S1): S63–S63, doi: 10.1121/1.1995349.
9. He C., Yang K., Lei B., Ma Y. (2015), Forward scattering detection of a submerged moving target based on the adaptive filtering technique, *Journal of Acoustical Society of America*, **138**(3): 293–298, doi: 10.1121/1.4929807.
10. He C., Yang K., Ma Y. (2016), Analysis of the arriving-angle structure of the forward scattered wave on a vertical array in shallow water, *Journal of the Acoustical Society of America*, **140**(3): 256–262, doi: 10.1121/1.4962338.
11. Herstein P.D., Cole B.F., Browning D.G., Groneman F.L. (2006), Sensitivity of shallow water transmission loss to source and receiver proximity to a hard bottom under downward refracting conditions, *Journal of the Acoustical Society of America*, **92**(4): 2302, doi: 10.1121/1.405129.
12. Jensen F.B., William A. Kuperman W.A., Porter M.B, Schmidt H. (2011), *Computational ocean acoustics*, Springer Science & Business Media, doi: 10.1007/978-1-4419-8678-8.
13. Katsnelson B.G, Petnikov V.G, Lynch J.F. (2001), Shallow Water Acoustics,*Journal of the Acoustical Society of America*, **112**(6): 2502–2504, doi: 10.1121/1.1518696.
14. Lei B., Yang K., Ma Y. (2012), Range estimation for forward scattering of an underwater object with experimental verification, *Journal of Acoustical Society of America*, **132**(4): 284–289, doi: 10.1121/1.4747273.
15. Lei B., Yang K., Ma Y. (2014), Forward scattering detection of a submerged object by a vertical hydrophone array, *Journal of the Acoustical Society of America*, **136**(6): 2998–3007, doi: 10.1121/1.4901709.
16. Lei Z., Yang K., Ma Y. (2016), Passive localization in the deep ocean based on the cross-correlation function matching, *Journal of the Acoustical Society of America*, **139**(6): 196–201, doi: 10.1121/1.4954053.
17. Sheng X., Lu J., Dong W., Yin J., Guo L., Wu X. (2014), The research on the coverage area of multistatic sonar in various working modes, *Proceedings of Meetings on Acoustics*, **21**(1): 070005, doi: 10.1121/1.4890017.
18. Urick R.J. (1965), Caustics and convergence zones in deep-water sound transmission, *Acoustical Society of America Journal*, **38**(2): 1191, doi: 10.1121/1.1939471.
19. Xia H., Yang K., Ma Y. (2016), Noise reduction method for acoustic sensor arrays in underwater noise, *IEEE Sensors Journal*, **16**(24): 8972–8981, doi: 10.1109/JSEN.2016.2618770.
20. Xiao P., Yang K. (2016), Model of shipping noise in the deep water: directional density and spatial coherence functions, *China Ocean Engineering*, **30**(4): 591–601, doi: 10.1007/s13344-016-0037-3.
21. Yang K., Li H., Duan R., Yang Q. (2017), Analysis on the characteristic of cross-correlated field and its potential application on source localization in deep water, *Journal of Computational Acoustics*, **25**(2): S1, doi: 10.1142/S0218396X17500011.
22. Yang K., Li H., He C., Duan R. (2016), Error analysis on bearing estimation of a towed array to a far-field source in deep water, *Acoustics Australia*, **44**(3): 429–437, doi: 10.1007/s40857-016-0070-7.
23. Yang K., Lu Y., Lei Z., Xia H. (2017), Passive localization based on multipath time-delay difference with two hydrophones in deep ocean, *Acoustics Australia*, **45**(4): 1–10, doi: 10.1007/s40857-017-0084-9.
24. Yang K., Ma Y., Sun C., Miller J.H., Potty G.R. (2004), Multi-step matched field inversion for broadband data from ASIAEX2001, *IEEE Journal of Oceanic Engineering*, **29**(4): 964–972, doi: 10.1109/JOE.2004.835211.
25. Yang K., Ross C., Ma Y. (2007), Estimating parameter uncertainties in Geoacoustic inversion by a neighbourhood algorithm, *Journal of Acoustical Society of America*, **121**(2): 833–843, doi: 10.1109/OCEANS.2006.306799.
26. Yang K., Yang Q., Duan R., Guo X., Cao R. (2016), A simple method for source depth estimation with multipath time delay in the deep ocean, *Chinese Physics Letters*, **33**(12): 124302, doi: 10.1088/0256-307X/33/12/124302.
27. Zhang T., Yang K., Ma Y., Wang Y. (2015), A robust localization method for source localization based on the auto-correlation function of wide-band signal, *Acta Physica Sinica*, **64**(2): 276–282, doi: 10.7498/aps.64.024303.
28. Zhang Z.Y. (2016), Analytical formulas for incoherent transmission loss in shallow water based on effective approximations of seafloor depth and reflectivity, *Journal of the Acoustical Society of America*, **140**, 3407, doi: 10.1121/1.4970942.
29. Zhao K., Liang J., Karlsson J., Li J. (2013), Enhanced multistatic active sonar signal processing, *Journal of the Acoustical Society of America*, **134**(1): 300–311, doi: 10.1121/1.4809648.